scientific reports

Check for updates

OPEN

Modulation of the northward penetration of Antarctica intermediate waters into the eastern equatorial Indian Ocean under glacial and interglacial conditions

Sandrine Le Houedec✉, Maxime Tremblin, Amaury Champion & Elias Samankassou

The Indo-Pacific warm pool is the warmest and most dynamic ocean–atmosphere-climate system on Earth and was subject to significant climate changes during the Pleistocene glacial-interglacial transitions. This has been shown to significantly affected the strength of surface waters that redistribute heat from the tropics to the southern part of the Indian Ocean. Here we investigate the response of the oceanic circulation at intermediate depth (1200 m) of the eastern equatorial Indian Ocean (EEIO) with neodymium (Nd) isotopes in the context of the climatic oscillation of the last 500 ka. The most striking feature of our new dataset is the seesaw Nd record that mimics glacial-interglacial cycles. While the interglacial periods are characterized by a higher contribution of the less radiogenic neodymium (~ − 7ε_{Nd}) Antarctic Intermediate Water (AAIW), the glacial periods are characterized by more radiogenic water mass of Pacific origin (~ − 5ε_{Nd}). To explain the increase in the ε_{Nd} signature toward a more radiogenic signature as the Indo-Pacific connection is reduced under the low sea level of the glacial periods, we show that under global cooling, the AAIW advances northward into the tropics, which is a consequence of the general slowdown of the thermohaline circulation. Therefore, oceanic mixing at intermediate depth in the eastern tropical Indian intermediate water is modulated by the production rate of the AAIW in the Southern Ocean. Our study provides new evidence for the role that changes in the deep oceanic conditions play in amplifying externally forced climate changes that ultimately lead to drier/moister atmospheric conditions and weaker/stronger monsoons during glacial/interglacial periods over eastern tropical Indian Ocean.

The East Equatorial Indian Ocean (EEIO) represents the western part of the larger Indo-Pacific Warm Pool (IPWP). This equatorial region holds a key position on the globe, characterized by sea surface temperature (SST) consistently above 28 °C[1] and strong rainfall, and contributes to the northward distribution of heat through high convective clouds[2]. The EEIO plays an active role in regulating global climate change[3,4] and has been classified as one of the major climate "hotspots" by the 5th and 6th successive IPCC reports[5–7]. Indeed, ocean–atmosphere processes are strongly coupled in this area, and despite relatively steady and warm SST, salinity varies considerably due to seasonal Australian-Indonesian monsoonal activity. Due to the central role of EEIO on the global thermohaline circulation, its property fluctuations (temperature and salinity) play an active role in regulating global oceanic dynamics, global energy transfers, and global and regional climate[2,8]. The intermediate water masses originating from the southern hemisphere are an essential component of the thermohaline circulation, and there is growing evidence that these water masses play a significant role in the climate regulation of the Indian Ocean[9–11]. As an example, the Antarctic Intermediate Water (AAIW) is thought to transmit climate anomalies (i.e. through thermohaline properties, nutrients and inorganic carbon) from the Southern Ocean to the low latitude thermocline via the so-called "oceanic tunnel"[12–14]. This term describes the intermediate water

Department of Earth Sciences, University of Geneva, Rue des Maraîchers 13, 1205 Geneva, Switzerland. ✉email: sandrine.lehouedec@unige.ch

level pathway where southern-sourced waters flow towards the tropics and mitigate the tropical SST[15–18]. Collectively these studies support the idea that the vigor of the AAIW is one of the control parameters of the EEIO climate variability, highlighting a direct and significant link between oceanic and atmospheric processes in this crucial area of the Earth's climate system.

It is well known that the EEIO experienced significant climate changes as response to the global Pleistocene glacial/interglacial cycles[19–21], with SST oscillating between 26 and 22 °C[22,23]. However, past changes in the intermediate circulation are far less well-documented than those of surface and deep water[24–27]. Moreover, most of the studies of the intermediate water circulation focus on the last glaciation and are mainly derived from the Atlantic Ocean[26,28,29] and the Pacific Ocean[30,31]. The response of the AAIW to climatic change remains still understudied, and while some studies suggest an increased northward penetration of the AAIW in those oceans over the last glacial period[29,31,32], others based on ε_{Nd} and Cd/Ca records did not identify such changes[33,34]. For the Indian Ocean, a few studies provide information on the AAIW dynamics and highlight an increased contribution of this current during the last deglaciation into the northern basins[9–11,27] but none investigate the AAIW dynamics for the pre-LGM period. In this study we generated a high-resolution Neodymium-based oceanographic record together along with climatic proxies ($\delta^{18}O$ and Mg/Ca) to reconstruct the coupled ocean–atmosphere response of the EEIO to the 100-ka eccentricity climatic cycles of the last 500 ka in the EEIO.

Oceanographical settings

The ODP Site 762 (Hole B) is located on the Exmouth Plateau in the Western Australian Margin (19°53′ S, 112°15′ E) and was drilled at intermediate ocean depth (water depth = 1360 m). The sedimentary succession is mainly composed of well-preserved carbonated oozes. The ages were calculated using the age-depth tie points of the stratigraphically integrated age model for the last 6 Ma of the site ODP 762 Hole B[35]. Currently, the main features of the surface circulation affecting the Exmouth plateau are the Indonesian Throughflow (ITF), the West Australian Current (WAC, > 400 m), and the Leeuwin Current (LC, > 200 m) (Fig. 1). The ITF consists of warm and low-salinity waters flowing from the Pacific Ocean into the Indian Ocean through the Indonesian pathway[36]. The ITF surface waters diverge westward into the South Equatorial Current (SEC) and southward along the coast of west Australia, forming the warm and low-salinity LC[36–38] (Fig. 1). In addition to the influence of the ITF flow, the strength of the LC is partly controlled by the Australian-Indonesian monsoonal activity[39]. The WAC originates in the southern Indian Ocean[36] and is a cold water mass that flows northward to join the SEC near the tropics. These surface currents associated with the counter Eastern Gyral Current (EGC) allow the settlement of warm and salty waters that constitute the Indian warm pool (Fig. 1). Associated to these surface currents, two intermediate water currents affect the Exmouth plateau and influence the water column stratification of the study site: the Indonesian Intermediate water (IIW) and the Antarctic Intermediate Water (AAIW). The sill depth between the Pacific and Indian oceans at around 1250 m (Leti Strait[40]), leads to water flow of Pacific origin at an

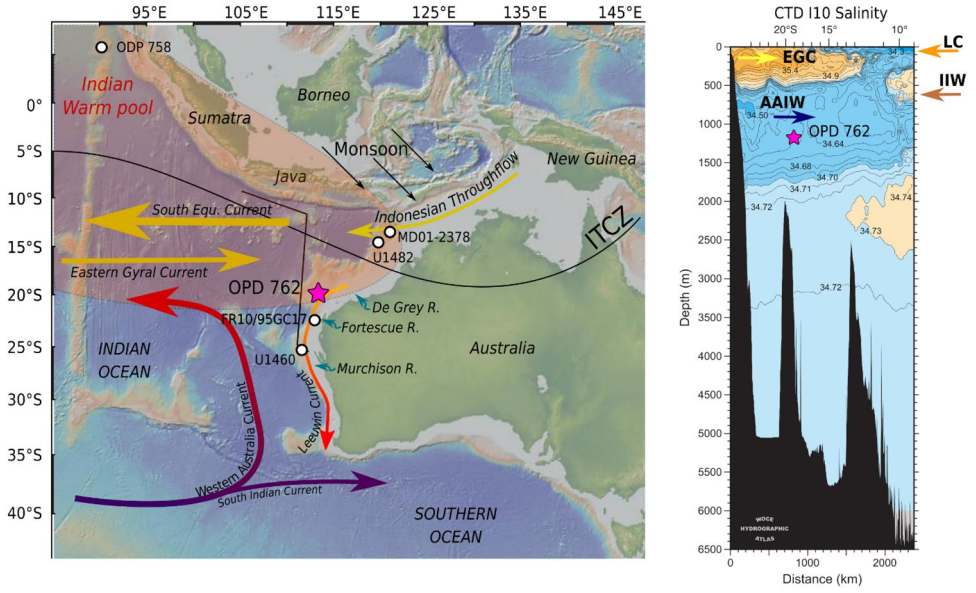

Figure 1. Main environmental and oceanographic features of the Equatorial East Indian Ocean. Left panel: Map that illustrates the surface currents in the EEIO. The pink star shows the current position of the study site ODP 762. Blue arrows show the outlet of the river near to the site ODP 762. The map was generated using map-based application GeoMapApp (http://www.geomapapp.org). Right panel: Salinity profile along CTD salinity profile I10 110° E (WOCE hydrographic surveys). The main water masses are marked: EGC, Eastern Gyral current; LC, Leeuwin current; IIW, Intermediate Indonesian Water; AAIW, Antarctic Intermediate Water. The Intertropical Convergence Zone (ITCZ) position corresponds to its Austral summer position (December -January).

intermediate depth, namely the IIW[41]. The AAIW originates around the Drake passage[42] and is characterized by a minimum salinity and flows below the subtropical gyre toward the study site (Fig. 1).

Results and discussion

Over the last 500 ka, our new multi-proxy data generated at the site ODP 762 follows the global glacial-interglacial (G-IG) climatic cyclicity. The sea surface temperature (SST) oscillates between 27 °C during IG and 23 °C during G (Fig. 2). On average, the SST range of variation is about 2.5 °C between successive G-IG episodes. The sea surface salinity (SSS) follows the G-IG cycles with overall rising SSS values over the glacial and decreasing values over the interglacial episodes and a range of variation at about 2.5 psu (from ~ 23.5 to ~ 26.5 ± 0.7 psu; Fig. 2). The Nd isotope values from the detrital component of the sediment vary from − 23.5 to − 19.5 ε_{Nd} with lower values reached during the IG and the highest values during the G (Fig. 2). The ε_{Nd} values of past seawater inferred range from − 8 to − 5 in a long-term increasing trend from 500 ka to modern time. This long-term trend is featured by embedded variations of 1.5–2 ε_{Nd} units that define the G-IG cycles (Fig. 3).

Enhanced river activity on the Western Australian margin under interglacial periods

The Western Australian margin is characterized by low salinity waters, which originate from the Indonesian archipelago through the Indonesian Throughflow (ITF) and local precipitation that freshen the surface layer along the pathway of the Leeuwin current[43] (LC). For instance, the southern position of the Intertropical Convergence Zone (ITCZ) during warm periods results in enhanced monsoonal activity in the area[44–48]. Additionally, sea level fluctuation in response to the G-IG cycles controls the water flux between the Pacific and the Indian Oceans which, in turn, control the strength of the ITF and the LC that carry warm and fresh waters along the western Australia margin[22,43,49] and even towards the western Indian margin[50]. The migration of salinity fronts

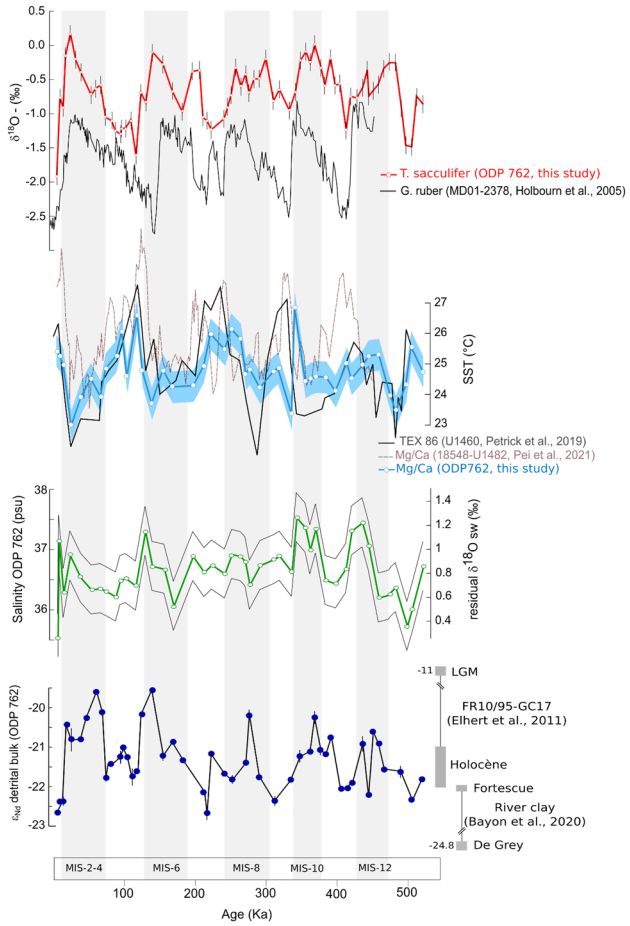

Figure 2. Hydrological and climatic evolution of the East Equatorial Indian Ocean over the last 500 ka. The grey bars highlight the glacial interval. From top to bottom: $\delta^{18}O$ evolution of *T. sacculifer* (in red) at site ODP 762 (this study) and *G. ruber* (in black) at site MD01-2378[60], SST evolution of the EEIO during the last 500 ka. TEX_{86} SST derived from the site U1460[23] (in black), and Mg/Ca temperatures derived from site 18548-U1482[22] (in red) and from site ODP 762 (in blue, this study), SSS evolution during the last 500 ka calculated from the equation $\delta^{18}O_{sw} = 0.54 \times S - 18.7$[61], and Nd isotopic composition from terrigenous phases of sites ODP 762 (this study) in the context of the Australian rivers Nd isotopic signatures.

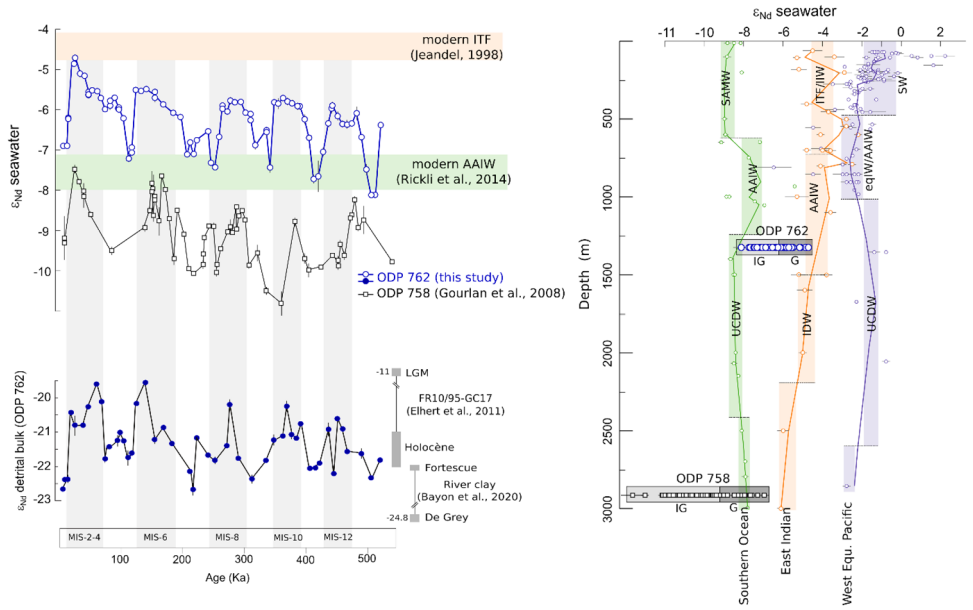

Figure 3. Compilation of regional Neodymium isotopic records. Left panel illustrates the Nd isotopic composition from both carbonate and terrigenous phases of sites ODP 762 (this study) and ODP 758[62]. Right panel shows the Nd isotopic composition of the modern ocean collected from GEOTRACEs database[75] for the Southern Ocean[70], East Indian Ocean[76,77] and West Equatorial Pacific Ocean[78,79]. The main water masses are marked: Subantarctic Mode Water (SAMW), Antarctic Intermediate Water (AAIW), Upper Circumpolar Deep Water (UCDW), Indonesian Throughflow and Intermediate Indonesian Water (ITF/IIW), Indian Deep Water (IDW), Surface Water (SW), Equatorial Intermediate Water (EQIW). Shadow area is the average ε_{Nd} value for each water mass.

is thus influenced by intricate interactions between ITF/LC dynamics and precipitation rates, both of which are modulated from seasonal to orbital scales[22,43,51].

In this study we used Nd and Sr isotopes to identify the provenance of the terrigenous fractions at Site ODP 762 (Fig. 1, Supplementary material Fig. S1) to monitor local river runoff and infer the monsoonal activity over the last 500 ka. The terrigenous sediment flux is thought to more directly capture the local monsoonal precipitation and runoff signal from the Australian continent[49,52]. Indeed, combinations of Nd, Sr, and Pb isotope ratios on the clay fractions at Site FR10/95-GC17 (Fig. 1), southeast of Site ODP 762, demonstrated that terrigenous particles in the area are predominantly riverine sources from west Australia during the warm Holocene[49]. In addition, eolian dust from north-western Australia should contribute little to the terrigenous fraction at Site ODP 762, as supported by the estimated terrigenous dust accumulation offshore north-western Australia[53]. We found that Nd isotope values of terrigenous particles during the IG periods are very close to the Nd isotope values of clay minerals from the nearby Fortescue and/or De Grey rivers (Fig. 1) with $\varepsilon_{Nd\text{-}clay} = -21.5$ and -23.4, respectively[54] indicating the western Australia river's origin of the terrigenous fractions at Site ODP 762 during the IG periods. The consistency of the Nd isotope values over the IG intervals suggests that the provenance of the terrigenous fractions at site ODP 762 has been relatively stable over interglacial intervals of the past 500 ka.

At site ODP 762, the drop in salinity occurred abruptly at the onset of most of the deglaciation events and is synchronous with a SST warming (Fig. 2, Supplementary material Fig. S2). These environmental changes are consistent with records from the nearby Core SO257-18571, where the drop in salinity and rise in SST at the termination has been attributed to the enhancement of "Ningaloo Niño"—type events[55] during the pCO_2 peak that follows glacial terminations[22]. These events trigger intense precipitation in the Indonesian region and western Australia[56] allowing large amounts of warm and fresh water to be transported along the western Australian margin through the LC. In this region, the hydrology cycle is known to follow precession cycle[57,58] but precipitation rate depend of ITCZ migration and sea level, which is slightly different for each climatic cycles[59]. Therefore, the weaker change in our salinity record for MIS8 might result of a less intense "Ningaloo Nino" type event at that time. In addition, we suggest that during deglaciation, those events of intense precipitation also trigger an increase in the western Australia river's activity, most likely through flash flood phenomena. The significant input of river water to the Ocean will enhance SSS freshening of the ITF/LC current. This hypothesis is supported by the ε_{Nd} record from the terrigenous particles at site ODP 762, which shows a sharp decrease in the ε_{Nd} values (from 1 to 2 ε_{Nd} units) at the glacial termination, confirming a massive release of particles from nearby rivers (Fig. 2). While not ruling out the primary role of the ITF/LC strength on SSS modulation, our data support the hypothesis of a non-negligible SSS control by local river activities. Therefore, combined with the intensification of the ITF under higher sea level stand, the reinforcement of the western Australian rivers' activity at the deglaciation will exert a positive feedback on the decreasing salinity of the surface waters. We suggest that it is the combination

of the two phenomena, ITF strength and river's activity, which might explain such a large drop of sea surface salinity observed at the climatic transition in the eastern equatorial Indian Ocean.

Modification of the Eastern Equatorial Indian water column structure over glacial-interglacial cycles

Our study supports an overall colder and saltier surface layer in the EEIO during glacial periods and a warmer and fresher surface layer during interglacial periods. The authigenic ε_{Nd} at site ODP 762 oscillates in response to the G/IG cycles, with the signature driven by radiogenic Pacific water during glacial periods and a signature driven by the less radiogenic Southern Ocean during interglacial periods (Fig. 3, Supplementary material Fig. S2). The ε_{Nd} signature is expected to shift to less radiogenic values during glacial periods due to reduced oceanic connections between the Pacific and the EEIO[23]. Although a tectonic closure of an oceanic passage could potentially increase water flux through a bottleneck effect[62,63], our isotopic analyses indicate that this is unlikely to occur in the studied area during glacial periods. Indeed, the analyses of Nd isotopes (and Sr isotopes, Supplementary material Fig. S1) in terrigenous particles are too negative ($\varepsilon_{Nd} = -20$ to -19, Fig. 3) to support the hypothesis of an increase in particle input from the Indonesian region during these periods (Sumatra/Banda clays[49] $\varepsilon_{Nd} = -13$ to -3). The strength of the northward penetration of the Southern Ocean AAIW into the EEIO in response to global climate resolves this Indo-Pacific ε_{Nd} conundrum. Over the last 40 ka, evidence of northward penetration of the AAIW of Southern Ocean origin was reported for the northern Bay of Bengal[64] and attributed to episodes of warming during the last deglaciation in Antarctica and the Southern Hemisphere[65]. This mechanism has been linked to the modulation of the sea-ice coverage[66,67]. Indeed, it was modelled that under a warming climate, the AAIW shift poleward together with the surface salinity minimum due to the retreating sea ice[67]. Our new ε_{Nd} results show that similar processes also occur on the eccentricity time scale. Thus, under warmer intervals, the low Antarctic sea-ice coverage enhances the stratification in the Southern Ocean which will promote the production of subsurface and intermediate water masses, including the AAIW and its northward penetration. Consequently, the strong signature of the AAIW from the Southern Ocean, represented by a less radiogenic ε_{Nd} signature, will dominate in the EEIO during these deglaciations. In stark contrast, reduced AAIW during glacial periods causes the influence of less radiogenic AAIW waters in the eastern Indian Ocean to decrease despite the constriction of the Indo-Pacific water flow. Thus, the seesaw trend in ε_{Nd} of the intermediate water is directly derived from the imbalance between AAIW and ITF/IIW in the intermediate oceanic mixing of the EEIO. Superimposed on this seesaw pattern, a long-term increase of the ε_{Nd} value is also observed throughout the last 500 ka. This trend reflects the overall global increase of the seawater ε_{Nd} relative to the present value since the Mid-Pleistocene transition[68] (MPT).

To further our understanding of the surface-to-bottom water column structure, we compared our record to the ε_{Nd} signature obtained from the deeper site[62] (ODP 758, 2925 mbsl), located northwest of our studied site (ninety East Ridge, 5°23′ N, 90°21′ E, Fig. 1). This deep site mimics the G/IG oscillation identified in our study (Fig. 3) showing that the deep current also responds to eccentricity climate cycles. This deep-water Nd record has been interpreted to reflect a weakening and/or less radiogenic Antarctic Bottom Water (AABW) during interglacials[11,69], which is today[34,70] between -6.0 and -7.8 ε_{Nd}, It was shown that reduce AABW under warming climate result of the melting of the sea ice cover off Antarctica in the Southern Oceans decreasing the surface density flux and thus causing change in the deep circulation[71,72]. This in turn implies that the strength of the North Atlantic Deep Water was stronger during the interglacial periods[71,73,74]. Collectively, these results reveal that the vertical structure of the water column has fundamentally changed during G-IG cycles in the EEIO, with a strong AAIW/weak AABW northward flux during interglacial, and weak AAIW/strong AABW northward flux during glacial (Fig. 4).

AAIW as a feedback control parameter on the regional climate

During glacial intervals, our results support the hypothesis of a drastically reduced production of AAIW in the Southern Ocean, which, in turn, hinders its penetration northwards into the tropical Indian Ocean. Moreover, we propose that the AAIW layer in the EEIO will undergoes significant thinning during glacial periods due to

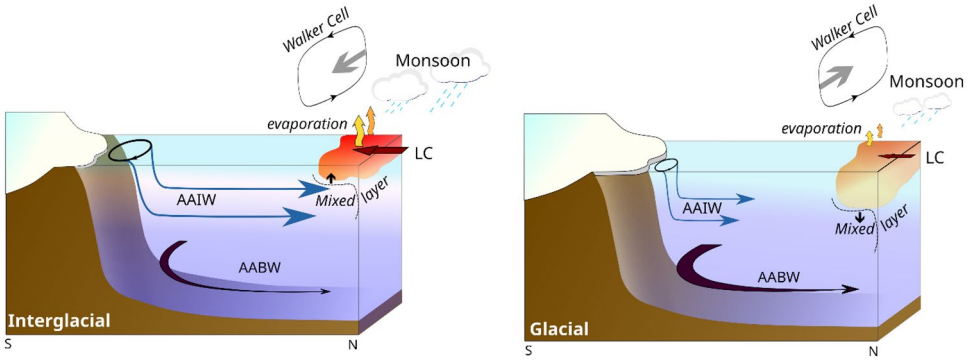

Figure 4. Scenarios of climatic and oceanographic behavior under glacial and interglacial conditions at the EEIO.

additional factors: (1) the deepening of the surface layer caused by increased density, resulting from colder and saltier surface water, and (2) the expansion of AABW volume due to a high production rate. Conversely, during interglacial periods, a shallower surface layer and weaker AABW will allow the AAIW to easily penetrate northward, resulting in a strong imprint of the AAIW into the Indian Ocean (Fig. 4). Today, the eastern tropical Indian Ocean experiences a strong upwelling of cool, nutrient-rich waters from deeper layers during the summer monsoon season[80,81]. Indeed, a shallower mixed layer allows more upwelling, which in turn intensifies the monsoon by enhancing the sea-air exchange. On a longer time scale, it has also been shown that the mixed layer was shallower along the Sumatra western coastline during the Holocene than during the Last Glacial Maximum[16]. Therefore, we suggest that under warming conditions, the strengthening of northwards flow of the AAIW into the EEIO will shallow the mixed layer depths, amplifying the ability of the surface layer to exchange heat and moisture with the atmosphere and, ultimately enhancing the activity of the Australian-Indonesian monsoon (Fig. 4). Conversely, under glacial conditions, the weak penetration of the AAIW into the EEIO, combined with a saltier surface layer, will deepen the mixed layer and reduce the efficiency of the ocean–atmosphere exchanges. In this scenario, the modulation of the AAIW flux penetrating the EEIO is a non-negligible parameter amplifying externally forced climate changes. In this context, exploring the behavior of the global intermediate oceanic layer during the Pleistocene climatic oscillation seems essential to fully understand the ocean–atmosphere coupling from which the specific spatial expression of global climatic changes is derived. Finally, our new results highlight the need to integrate an intermediate oceanic layer into numerical simulation in order to complete our understanding of the response of the monsoon activity in the context of ongoing global climate change.

Methods

Nd measurements

The Nd isotopic data of ancient seawater was obtained from leachates of carbonate bulk samples (400 mg). In the studied area, it was shown that the acetic acid dissolution (1.6 N) of bulk sediment gave the same results as measurements done on isolated foraminifera due to the high $CaCO_3$ content (> 85%) of the samples[62,63,82]. Neodymium has been separated using two ion chromatography columns[83] using Eichrom TRU-Spec™ resin and the Eichrom LnSpec™ resin. The entire procedure Nd blanks were monitored to be smaller than 2 pg and thus is negligible compared to the Nd content of samples (around 1000 ppm). Nd isotopic ratios were measured on a Neptune MC-ICP-MS (Thermo Finnigan). The Nd isotopic results are expressed in ε_{Nd} as:

$$\varepsilon_{Nd} = \left[\left({}^{143}Nd/{}^{144}Nd_{sample}\right)/\left({}^{143}Nd/{}^{144}Nd_{CHUR}\right) - 1\right] * 10000$$

with ${}^{143}Nd/{}^{144}Nd_{CHUR}$[84] = 0.512638.

The average external reproducibility of the Nd isotopic measurements was monitored by multiple analyses of NIST 3135 A standard (${}^{143}Nd/{}^{144}Nd$ of 0.511411; $2\sigma = 7 \times 10^{-6}$; n = 206). The accuracy on ε_{Nd} is calculated to ± 0.2 (2σ). The residual fraction was leached and rinsed by an alternation of three distilled-water rinses and two HBr (1 N) leaches to provide detrital fractions cleaned from residual carbonate and/or Fe–Mn oxides[85]. Then, the fractions were first dissolved by a mixture of distilled HNO_3 (16 N) and HF (27 N, 0.5 mL for 50 mg) on a hot plate for 24 h, then evaporated. The residual materials were dissolved again using HNO_3 (16 N), and purified H_3BO_3 (9 N, for Sr) was added to remove CaF_2 crystals[85]. Nd and Sr isotopes of the detrital component were purified on columns from this final solution[86].

Mg/Ca measurements

Between 25 and 30 shells of *Trilobus sacculifer* were handpicked and cleaned following the procedure of Barker et al., 2003. The shells were gently crushed using two clean glass plates to open the chambers, then they were cleaned using successive baths of double-distilled water (DDW), glacial ethanol, and alkali buffered 1% H_2O_2 in an ultrasonic bath to remove successively clays and organic matter. A final weak acid leach was done using 0.001 M HNO_3 to remove any adsorbed contaminants from the test fragments. The Mg/Ca ratio was measured on an iCAP 6000 ICP–OES at the University of Geneva. Both Mg and Ca were radially measured on 280.270 and 317.933 nm, respectively. Each single Mg/Ca ratio is the average of three measurements from which the analytical errors are deduced. Mg/Ca ratios were normalized to the JCP-1 certified material[87]. The external reproducibility was obtained using replicate samples with an average standard deviation of 0.024 mmol/mol and measurements of multiples. JCP-1 standard solutions at concentrations similar to those of the measured samples give Mg/Ca = 4.199 ± 0.02 mmol/mol (2σ, n = 42). The sea surface temperature (SST) was obtained from *T. sacculifer* Mg/Ca ratios using MgCarb software[88], currently recognized to be the best method to obtain accurate temperature from Mg/Ca measurements of foraminiferal shells[89].

$\delta^{18}O$ measurements

$\delta^{18}O$ was analyzed on a mix of 5–7 shells of *T. sacculifer* (without the last chamber). Shells were handpicked in the size fraction of 300–400 µm and cleaned in DDW in an ultrasonic bath to remove nannofossil oozes and clays. The $\delta^{18}O$ values were determined from the CO_2 extracted at 90 °C on an ISOCARB™ device on-line with a VG-PRISM™ mass spectrometer at GEOTOP laboratory at the University of Montréal (UQAM). The values are expressed against the V-PDB standard. The overall analytical reproducibility, as calculated from replicate measurements on the in-house reference standard carbonate material ($\delta^{18}O = -1.30‰$) normalized to the VSMOW-SLAP with a reproducibility of ± 0.05‰ (± 1 s). Sea surface salinity (SSS) was derived from *T. sacculifer* $\delta^{18}O$ measurements ratios. The $\delta^{18}O$ of seawater was calculated from $\delta^{18}O$ of foraminiferal calcite and Mg/Ca-based temperature estimates of *T. sacculifer* based on the equation established for this species[90]. Then, we corrected this calculated $\delta^{18}O$ seawater value from the global seawater value[91] to account for the ice volume with a cumulative

error estimation of $\delta^{18}O_{sw}$ of ~ 0.25‰. The residual $\delta^{18}O$ signal was used to calculate the salinity using the $\delta^{18}O_{sw}$–salinity relationship[92].

Data availability

The dataset generated for the current study is available in the PANGEA repository: https://doi.org/https://doi.org/10.1594/PANGAEA.96092.

Received: 26 May 2023; Accepted: 18 March 2024
Published online: 20 March 2024

References

1. Yan, X.-H., Ho, C.-R., Zheng, Q. & Klemas, V. Temperature and size variabilities of the Western Pacific warm pool. *Science* **258**, 1643–1645 (1992).
2. Ganachaud, A. & Wunsch, C. Improved estimates of global ocean circulation, heat transport and mixing from hydrographic data. *Nature* **408**, 453–457 (2000).
3. DiNezio, P. N. *et al.* Glacial changes in tropical climate amplified by the Indian Ocean. *Sci. Adv.* **4**, eaat9658 (2018).
4. Saji, N. H., Goswami, B. N., Vinayachandran, P. N. & Yamagata, T. A dipole mode in the tropical Indian Ocean. *Nature* **401**, 360–363 (1999).
5. Giorgi, F. Climate change hot-spots. *Geophys. Res. Lett.* **33**, 8 (2006).
6. Masson-Delmotte, V. *et al. IPCC, 2021: Climate Change 2021: The Physical Science Basis. Contribution of Working Group I to the Sixth Assessment Report of the Intergovernmental Panel on Climate Change*. https://doi.org/10.1017/9781009157896. (2021).
7. Turco, M., Palazzi, E., von Hardenberg, J. & Provenzale, A. Observed climate change hotspots. *Geophys. Res. Lett.* **42**, 3521–3528 (2015).
8. Macdonald, A. M. & Wunsch, C. An estimate of global ocean circulation and heat fluxes. *Nature* **382**, 436–439 (1996).
9. Jung, S. J. A., Kroon, D., Ganssen, G., Peeters, F. & Ganeshram, R. Enhanced Arabian Sea intermediate water flow during glacial North Atlantic cold phases. *Earth Planet. Sci. Lett.* **280**, 220–228 (2009).
10. Ma, R. *et al.* Changes in intermediate circulation in the Bay of Bengal since the last glacial maximum as inferred from benthic Foraminifera assemblages and geochemical proxies. *Geochem. Geophys. Geosyst.* **20**, 1592–1608 (2019).
11. Yu, Z. *et al.* Antarctic Intermediate Water penetration into the Northern Indian Ocean during the last deglaciation. *Earth Planet. Sci. Lett.* **500**, 67–75 (2018).
12. Liu, Z. & Yang, H. Extratropical control of tropical climate, the atmospheric bridge and oceanic tunnel. *Geophys. Res. Lett.* **30**, 5 (2003).
13. Pena, L. D. *et al.* Rapid changes in meridional advection of Southern Ocean intermediate waters to the tropical Pacific during the last 30kyr. *Earth Planet. Sci. Lett.* **368**, 20–32 (2013).
14. Romahn, S., Mackensen, A., Groeneveld, J. & Pätzold, J. Deglacial intermediate water reorganization: New evidence from the Indian Ocean. *Clim. Past* **10**, 293–303 (2014).
15. Kiefer, T., McCave, I. N. & Elderfield, H. Antarctic control on tropical Indian Ocean sea surface temperature and hydrography. *Geophys. Res. Lett.* **33**, 24 (2006).
16. Mohtadi, M. *et al.* Late Pleistocene surface and thermocline conditions of the eastern tropical Indian Ocean. *Quat. Sci. Rev.* **29**, 887–896 (2010).
17. Naidu, P. D. & Govil, P. New evidence on the sequence of deglacial warming in the tropical Indian Ocean. *J. Quat. Sci.* **25**, 1138–1143 (2010).
18. Visser, K., Thunell, R. & Stott, L. Magnitude and timing of temperature change in the Indo-Pacific warm pool during deglaciation. *Nature* **421**, 152–155 (2003).
19. De Deckker, P., Moros, M., Perner, K. & Jansen, E. Influence of the tropics and southern westerlies on glacial interhemispheric asymmetry. *Nat. Geosci.* **5**, 266–269 (2012).
20. Lea, D. W., Pak, D. K. & Spero, H. J. Climate impact of late quaternary equatorial pacific sea surface temperature variations. *Science* **289**, 1719–1724 (2000).
21. Russell, J. M. *et al.* Glacial forcing of central Indonesian hydroclimate since 60,000 y B.P.. *Proc. Natl. Acad. Sci.* **111**, 5100–5105 (2014).
22. Pei, R. *et al.* Evolution of sea surface hydrology along the Western Australian margin over the past 450 kyr. *Paleoceanogr. Paleoclimatol.* **36**, e2021PA004222 (2021).
23. Petrick, B. *et al.* Glacial Indonesian throughflow weakening across the Mid-Pleistocene Climatic transition. *Sci. Rep.* **9**, 16995 (2019).
24. Kallel, N., Labeyrie, L. D., Juillet-Leclerc, A. & Duplessy, J.-C. A deep hydrological front between intermediate and deep-wafpr, masses in the glacial Indian Ocean. *Nature* **333**, 651–655 (1988).
25. Mix, A. C. & Fairbanks, R. G. North Atlantic surface-ocean control of Pleistocene deep-ocean circulation. *Earth Planet. Sci. Lett.* **73**, 231–243 (1985).
26. Oppo, D. W. & Fairbanks, R. G. Variability in the deep and intermediate water circulation of the Atlantic Ocean during the past 25,000 years: Northern Hemisphere modulation of the Southern Ocean. *Earth Planet. Sci. Lett.* **86**, 1–15 (1987).
27. Waelbroeck, C. *et al.* Distant origin of circulation changes in the Indian Ocean during the last deglaciation. *Earth Planet. Sci. Lett.* **243**, 244–251 (2006).
28. Lynch-Stieglitz, J. *et al.* Atlantic meridional overturning circulation during the last glacial maximum. *Science* **316**, 66–69 (2007).
29. Pahnke, K., Goldstein, S. L. & Hemming, S. R. Abrupt changes in Antarctic Intermediate Water circulation over the past 25,000 years. *Nat. Geosci.* **1**, 870–874 (2008).
30. Bostock, H. C., Opdyke, B. N. & Williams, M. J. M. Characterising the intermediate depth waters of the Pacific Ocean using δ13C and other geochemical tracers. *Deep Sea Res. Part I: Oceanogr. Res. Pap.* **57**, 847–859 (2010).
31. Pahnke, K. & Zahn, R. Southern hemisphere water mass conversion linked with North Atlantic climate variability. *Science* **307**, 1741–1746 (2005).
32. Dubois-Dauphin, Q. *et al.* South Atlantic intermediate water advances into the North-east Atlantic with reduced Atlantic meridional overturning circulation during the last glacial period. *Geochem. Geophys. Geosyst.* **17**, 2336–2353 (2016).
33. Came, R. E., Oppo, D. W., Curry, W. B. & Lynch-Stieglitz, J. Deglacial variability in the surface return flow of the Atlantic meridional overturning circulation. *Paleoceanography* **23**, 1 (2008).
34. Howe, J. N. W. *et al.* Antarctic intermediate water circulation in the South Atlantic over the past 25,000 years. *Paleoceanography* **31**, 1302–1314 (2016).
35. Auer, G., De Vleeschouwer, D. & Christensen, B. A. Toward a Robust Plio-Pleistocene Chronostratigraphy for ODP Site 762. *Geophys. Res. Lett.* **47**, e2019GL085198 (2020).
36. Tomczak, M. & Godfrey, S. J. *Regional Oceanography: An Introduction* (Springer, 2001).

37. Atmadipoera, A. *et al.* Characteristics and variability of the Indonesian throughflow water at the outflow straits. *Deep Sea Res. Part I: Oceanogr. Res. Pap.* **56**, 1942–1954 (2009).
38. Woo, M. & Pattiaratchi, C. Hydrography and water masses off the western Australian coast. *Deep Sea Res. Part I: Oceanogr. Res. Pap.* **55**, 1090–1104 (2008).
39. Ridgway, K. R. & Condie, S. A. The 5500-km-long boundary flow off western and southern Australia. *J. Geophys. Res.: Oceans* **109**, 4 (2004).
40. Van Bennekom, A. J. Deep-water transit times in the eastern Indonesian basins, calculated from dissolved silica in deep and interstitial waters. *Netherl. J. Sea Res.* **22**, 341–354 (1988).
41. Talley, L. D. & Sprintall, J. Deep expression of the Indonesian Throughflow: Indonesian intermediate water in the south Equatorial Current. *J. Geophys. Res.: Oceans* **110**, 10 (2005).
42. Talley, L. D. Antarctic intermediate water in the South Atlantic. In *The South Atlantic: Present and Past Circulation* (eds. Wefer, G. *et al.*) 219–238 (Springer, 1996). https://doi.org/10.1007/978-3-642-80353-6_11.
43. Zhang, N., Feng, M., Du, Y., Lan, J. & Wijffels, S. E. Seasonal and interannual variations of mixed layer salinity in the southeast tropical Indian Ocean. *J. Geophys. Res.: Oceans* **121**, 4716–4731 (2016).
44. Broccoli, A. J., Dahl, K. A. & Stouffer, R. J. Response of the ITCZ to Northern Hemisphere cooling. *Geophys. Res. Lett.* **33**, 1 (2006).
45. Kang, S. M., Held, I. M., Frierson, D. M. W. & Zhao, M. The response of the ITCZ to extratropical thermal forcing: idealized slab-ocean experiments with a GCM. *J. Clim.* **21**, 3521–3532 (2008).
46. Mohtadi, M., Prange, M. & Steinke, S. Palaeoclimatic insights into forcing and response of monsoon rainfall. *Nature* **533**, 191–199 (2016).
47. Schneider, T., Bischoff, T. & Haug, G. H. Migrations and dynamics of the intertropical convergence zone. *Nature* **513**, 45–53 (2014).
48. Yan, M., Wang, B. & Liu, J. Global monsoon change during the Last Glacial Maximum: A multi-model study. *Clim. Dyn.* **47**, 359–374 (2016).
49. Ehlert, C. *et al.* Current transport versus continental inputs in the eastern Indian Ocean: Radiogenic isotope signatures of clay size sediments. *Geochem. Geophys. Geosyst.* **12**, 6 (2011).
50. Nuber, S. *et al.* Indian Ocean salinity build-up primes deglacial ocean circulation recovery. *Nature* **617**, 306–311 (2023).
51. Hu, S. *et al.* Interannual to decadal variability of upper-Ocean Salinity in the Southern Indian Ocean and the role of the Indonesian throughflow. *J. Clim.* **32**, 6403–6421 (2019).
52. Milliman, J. D. & Farnsworth, K. L. *River Discharge to the Coastal Ocean: A Global Synthesis* (Cambridge University Press, 2011). https://doi.org/10.1017/CBO9780511781247.
53. Kuhnt, W. *et al.* Southern Hemisphere control on Australian monsoon variability during the late deglaciation and Holocene. *Nat. Commun.* **6**, 5916 (2015).
54. Bayon, G. *et al.* Rare earth element and neodymium isotope tracing of sedimentary rock weathering. *Chem. Geol.* **553**, 119794 (2020).
55. Feng, M., McPhaden, M. J., Xie, S.-P. & Hafner, J. L. Niña forces unprecedented Leeuwin Current warming in 2011. *Sci. Rep.* **3**, 1277 (2013).
56. Su, L., Du, Y., Feng, M. & Li, J. Ningaloo Niño/Niña and their regional climate impacts as recorded by corals along the coast of Western Australia. *Palaeogeogr. Palaeoclimatol. Palaeoecol.* **535**, 109368 (2019).
57. Tachikawa, K. *et al.* The precession phase of hydrological variability in the Western Pacific Warm Pool during the past 400 ka. *Quat. Sci. Rev.* **30**, 3716–3727 (2011).
58. Wang, Y. *et al.* Millennial- and orbital-scale changes in the East Asian monsoon over the past 224,000 years. *Nature* **451**, 1090–1093 (2008).
59. Wang, G. *et al.* Precipitation variations of western equatorial pacific during glacial–interglacial cycles since MIS8: Evidence from multi–proxies of abyssal sediment. *Front. Earth Sci.* **10**, 369 (2023).
60. Holbourn, A. *et al.* Orbitally paced paleoproductivity variations in the Timor Sea and Indonesian Throughflow variability during the last 460 kyr. *Paleoceanography* **20**, 3 (2005).
61. Kim, Y., Rho, T. & Kang, D.-J. Oxygen isotope composition of seawater and salinity in the western Indian Ocean: Implications for water mass mixing. *Mar. Chem.* **237**, 104035 (2021).
62. Gourlan, A. T., Meynadier, L. & Allègre, C. Tectonically driven changes in the Indian Ocean circulation over the last 25Ma: Nd-isotope evidence. *Earth. Planet. Sci. Lett.* **267**, 353–364 (2008).
63. Le Houedec, S., Meynadier, L. & Allègre, C. Nd isotopic systematics on ODP Sites 756 and 762 sediments reveal major volcanic, oceanic and climatic changes in South Indian Ocean over the last 35 Ma. *Earth. Planet. Sci. Lett.* **327–328**, 29–38 (2012).
64. Ma, Y. *et al.* Strong Southern African Monsoon and weak Mozambique Channel throughflow during Heinrich events: Implication for Agulhas leakage. *Earth Planet. Sci. Lett.* **574**, 117148 (2021).
65. Masson-Delmotte, V. *et al.* EPICA Dome C record of glacial and interglacial intensities. *Quat. Sci. Rev.* **29**, 113–128 (2010).
66. Shemesh, A. *et al.* Sequence of events during the last deglaciation in Southern Ocean sediments and Antarctic ice cores. *Paleoceanography* **17**, 1–7 (2002).
67. Li, L., Liu, Z., Zhu, C., He, C. & Otto-Bliesner, B. Shallowing glacial Antarctic intermediate water by changes in sea ice and hydrological cycle. *Geophys. Res. Lett.* **48**, e2021GL094317 (2021).
68. Tachikawa, K., Rapuc, W., Dubois-Dauphin, Q., Guihou, A. & Skonieczny, C. Reconstruction of Ocean circulation based on neodymium isotopic composition: Potential limitations and application to the mid-pleistocene transition. *Oceanography* **33**, 2 (2020).
69. Bang, S. *et al.* Deep-water circulation over the last two glacial cycles reconstructed from authigenic neodymium isotopes in the equatorial Indian Ocean (Core HI1808-GPC04). *Ocean Sci. J.* **57**, 324–333 (2022).
70. Rickli, J. *et al.* Neodymium and hafnium boundary contributions to seawater along the West Antarctic continental margin. *Earth Planet. Sci. Lett.* **394**, 99–110 (2014).
71. Shin, S.-I., Liu, Z., Otto-Bliesner, B. L., Kutzbach, J. E. & Vavrus, S. J. Southern Ocean sea-ice control of the glacial North Atlantic thermohaline circulation. *Geophys. Res. Lett.* **30**, 2 (2003).
72. Govin, A. *et al.* Evidence for northward expansion of Antarctic Bottom Water mass in the Southern Ocean during the last glacial inception. *Paleoceanography* **24**, 1 (2009).
73. Brix, H. & Gerdes, R. North Atlantic Deep Water and Antarctic Bottom Water: Their interaction and influence on the variability of the global ocean circulation. *J. Geophys. Res.: Oceans* **108**, 2 (2003).
74. Crowley, T. J. North Atlantic Deep Water cools the southern hemisphere. *Paleoceanography* **7**, 489–497 (1992).
75. van de Flierdt, T. *et al.* Neodymium in the oceans: A global database, a regional comparison and implications for palaeoceanographic research. *Philos. Trans. R. Soc. A: Math. Phys. Eng. Sci.* **374**, 20150293 (2016).
76. Amakawa, H., Sotto-Alibo, D. & Nozaki, Y. Nd isotopic composition and REE pattern in the surface waters of the eastern Indian Ocean and its adjacent seas. *Geochim. Cosmochim. Acta* **64**, 1715–1727 (2000).
77. Jeandel, C., Thouron, D. & Fieu, M. Concentrations and isotopic compositions of neodymium in the eastern Indian Ocean and Indonesian straits. *Geochim. Cosmochim. Acta* **62**, 2597–2607 (1998).
78. Grenier, M. *et al.* From the subtropics to the central equatorial Pacific Ocean: Neodymium isotopic composition and rare earth element concentration variations. *J. Geophys. Res. (C Oceans)* **118**, 592–618 (2013).
79. Lacan, F. & Jeandel, C. Tracing Papua New Guinea imprint on the central Equatorial Pacific Ocean using neodymium isotopic compositions and Rare Earth Element patterns. *Earth. Planet. Sci. Lett.* **186**, 497–512 (2001).

80. You, Y. & Tomczak, M. Thermocline circulation and ventilation in the Indian Ocean derived from water mass analysis. *Deep Sea Res. Part I: Oceanogr. Res. Pap.* **40**, 13–56 (1993).
81. Purba, N. P., Pranowo, W. S., Ndah, A. B. & Nanlohy, P. Seasonal variability of temperature, salinity, and surface currents at 0° latitude section of Indonesia seas. *Reg. Stud. Mar. Sci.* **44**, 101772 (2021).
82. Le Houedec, S., Meynadier, L. & Allègre, C. J. Seawater Nd isotope variation in the Western Pacific Ocean since 80 Ma (ODP 807, Ontong Java Plateau). *Mar. Geol.* **380**, 138–147 (2016).
83. Caro, G., Bourdon, B., Birck, J. L. & Moorbath, S. High-precision 142Nd/144Nd measurements in terrestrial rocks: Constraints on the early differentiation of the Earth's mantle. *Geochim. Cosmochim. Acta* **70**, 164–191 (2006).
84. Jacobsen, S. B. & Wasserburg, G. J. Sm-Nd isotopic evolution of chondrites. *Earth. Planet. Sci. Lett.* **50**, 139–155 (1980).
85. Bayon, G. *et al.* An improved method for extracting marine sediment fractions and its application to Sr and Nd isotopic analysis. *Chem. Geol.* **187**, 179–199 (2002).
86. Pin, C. & Bassin, C. Evaluation of a strontium-specific extraction chromatographic method for isotopic analysis in geological materials. *Anal. Chim. Acta* **269**, 249–255 (1992).
87. Okai, T., Suzuki, A., Kawahata, H., Terashima, S. & Imai, N. Preparation of a new geological survey of Japan geochemical reference material: Coral JCp-1. *Geostandards Newsl.* **26**, 95–99 (2002).
88. Gray, W. R. & Evans, D. Nonthermal influences on Mg/Ca in planktonic foraminifera: A review of culture studies and application to the last glacial maximum. *Paleoceanogr. Paleoclimatol.* **34**, 306–315 (2019).
89. Rosenthal, Y., Bova, S. & Zhou, X. A user guide for choosing planktic foraminiferal Mg/Ca-temperature calibrations. *Paleoceanogr. Paleoclimatol.* **37**, e2022PA004413 (2022).
90. Spero, H. J., Mielke, K. M., Kalve, E. M., Lea, D. W. & Pak, D. K. Multispecies approach to reconstructing eastern equatorial Pacific thermocline hydrography during the past 360 kyr. *Paleoceanography* **18**, 1 (2003).
91. de Boer, B., Lourens, L. J. & van de Wal, R. S. W. Persistent 400,000-year variability of Antarctic ice volume and the carbon cycle is revealed throughout the Plio-Pleistocene. *Nat. Commun.* **5**, 2999 (2014).
92. Weldeab, S., Schneider, R. R. & Kölling, M. Deglacial sea surface temperature and salinity increase in the western tropical Atlantic in synchrony with high latitude climate instabilities. *Earth Planet. Sci. Lett.* **241**, 699–706 (2006).

Acknowledgements

This study was funded by the University of Geneva (S18173) and the CNRS-INSU SYSTER program. We would like to thank the ICP centre and Dr. Sophie Michalet for the measurements at the University of Geneva. This work utilized samples provided by the International Ocean Discovery Program (IODP) and we warmly thank the staff of the Kochi Core Center for the sampling.

Author contributions

S. L. H. designed the study and performed all the analyses. S. L. H. and M. T. wrote the manuscript with inputs of all the co-authors. A. C. provided assistance during hand-picking and cleaning of foraminifera. In addition to help in the writing process, E. S. acquires the financial support for the study.

Competing interests

The authors declare no competing interests.

Additional information

Supplementary Information The online version contains supplementary material available at https://doi.org/10.1038/s41598-024-57411-5.

Correspondence and requests for materials should be addressed to S.H.